https://doi.org/10.48048/tis.2022.5813

Numerical Analysis of High Speed Flow Applications using Various Flux Schemes

Mithun Krishnan, Anurag Ray and Ravi Peetala*

Department of Mechanical Engineering, Visvesvaraya National Institute of Technology, Nagpur 440010, India

(*Corresponding author's email: rkpeetala@mec.vnit.ac.in)

Received: 10 August 2021, Revised: 26 October2021, Accepted: 31 October2021

Abstract

Numerical analysis using computational fluid dynamics is an affordable and effective method with increasing relevance every day in research and engineering problems. Choosing an appropriate convective discretization scheme is paramount importance for obtaining more accurate solutions using CFD methods. The present study compares two commonly used numerical convective schemes, the upwind scheme of Advection Upstream Splitting Method (AUSM) and the central schemes of Kurganov-Noelle-Petrova and Kurganov-Tadmor scheme (K-T) have been made to find the better central scheme. These two schemes are validated with inviscid 1D and 2D problems such as Sod's shock tube, forward facing step in a Mach 3 tunnel, 15 Degree ramp in a Mach 2 supersonic tunnel, the Mach-reflection problem and scramjet engine operating under high Mach number. The AUSM and K-T schemes are robust enough to capture all the features of compressible flows. Comparison of results obtained by these 2 schemes is presented using density contours and surface property changes. It has been observed that both the schemes are robust enough to capture the flow features of the problems and that they have better accuracy for different conditions.

Keywords: OpenFOAM, AUSM, Kurganov-Tadmor, Convective discretization schemes, Supersonic flow

Introduction

Man has always been fascinated by the idea of flight and from the first practical airplane of The Wright Brothers in 1903, 1 thing has always been the driving force - to fly higher and faster. Advancements in aircrafts since then have been rapid and now even the extreme high-speed end of the flight spectrum has been explored and utilized [1]. For conducting tests in high-speed flow, experimental investigations would have a very high initial and operating cost. In modern times, with increasing computational capability, easier problem modification, lesser costs and adequate reliability, numerical techniques are preferred for carrying out these investigations. The key to producing accurate numerical solutions to aerodynamic problems is the usage of proper numerical schemes which can accurately capture all the changes occurring in the flow. This includes discontinuities like shock structures, mach reflection, mach stem, etc and hence the effciency of a scheme in obtaining these results plays a huge part in their selection. As such, 2 effective methods for convective scheme discretization are upwinding scheme and central differencing schemes. From the numerical studies performed [2], it was found that the Advection Upstream Splitting Method (AUSM) is simple, effective upwind scheme which had the highest accuracy [3]. Two effcient schemes are Kurganov-Noelle-Petrova (KNP) and Kurganov-Tadmor (KT) [4-6] schemes using the Van-Leer flux limiter [7]. However, no literature is available for a comparison between these 2 schemes.

Hence, in this study, a comparison between these 2 schemes shall be made to assess the robustness and accuracy of these 2 schemes by simulating simple inviscid problems 4 of which are in the supersonic regime and one in the hypersonic regime. The problems are solved using commercial codes for AUSM, available in ANSYS Fluent 16.0 and using rhoCentralFoam solver in the open-source software OpenFOAM version 3.0.1 for KNP and K-T scheme [4]. The results obtained are compared with those in works carried out by John [2]; Sod [8]; Woodward and Colella [9]; Ganesh [10]. In this work, first, a comparison is carried out between the central differencing scheme, after which the better one in rhoCentralFoam is compared with the AUSM scheme. The final objective of this study is to determine which the better scheme is so that future studies may be extended to cases involving hypersonic flow.

Governing equations

The governing equations are mathematical descriptions for fluid flow. These equations can be integral or differential based upon model of formulation and choice of control volume. In Computational Fluid Dynamics, these governing equations are discretized and converted into algebraic equations which can be solved subsequently with the help of the computer to determine the solution to a particular problem [1]. The set of governing equations in conservative differential form required to fully determine the solution is described in this section.

Conservation of mass

$$\frac{\partial \rho}{\partial t} + \nabla[u\rho] = 0 \tag{1}$$

Conservation of momentum

$$\frac{\partial (\rho u)}{\partial t} + \nabla[u(\rho u)] + \nabla p + \nabla . T = 0 \tag{2}$$

Conservation of total energy

$$\frac{\partial (\rho E)}{\partial t} + \nabla[u(\rho E)] + \nabla[\mathrm{u}p] + \nabla[T.u] + \nabla . j = 0 \tag{3}$$

where, T is the Viscous Stress Tensor Matrix, which is positive in Compression.

In high enthalpy hypersonic applications, N_2 and O_2 present in the air undergo chemical reactions due to high temperatures in the flow-field. But before reactions can occur, the di-atomic species vibrate rigorously about its mean position activating vibrational internal modes of energy. To capture all these effects additional equations are to be added to the developed solver for compressible flows. These extra equations are described next.

Landau-Teller vibrational relaxation equation

$$\frac{\partial (\rho evib_i)}{\partial t} + \nabla(evib_i) + \nabla(\rho_i U_i evib_i) = \frac{\rho c_i}{\tau_i}(evib_i{}^{eq} - evib_i) + R_i evib_i \tag{4}$$

Here, R_i is species production/destruction rate, $\rho ci = \rho i$, U_i is diffusion velocity given by Fick's Law (similar to Fourier's law of heat conduction), $evib_i$ is actual vibrational energy in the flow field of the individual di-atomic species. τ_i is relaxation time of individual species. (e.g. N^2, O^2 and NO), $evib_i{}^{eq}$ is equilibrium vibrational energy calculated by considering the translational temperature (e_{trans} = 0.5 fRT) [f = degrees of freedom (5 for di-atomic species)] [1]. The expression for relaxation rates is given by the following expression:

$$\tau_i = \frac{\tau_i}{p} e^{\left(\frac{c_2}{T}\right)^{1/3}} \tag{5}$$

Equilibrium vibrational energy mode is given by following expression. In the present study, the vibrating molecules are harmonic oscillators which follow Boltzmann's law of distribution among the quantized energy levels. C_1 and C_2 are gas specific and their values are provided in **Table 1**.

$$evib_i{}^{eq} = \frac{\frac{hv_i}{kT}}{e^{\frac{hv_i}{kT}} - 1} R_i T \tag{6}$$

In the equation above, h is Planck's constant, k is the Boltzmann constant, v_i is the fundamental node of vibrational frequency (**Table 2**), R_i is the characteristic gas constant and T is the translational temperature.

Table 1 Vibrational relaxation time constants.

Species	C_1 (μs-atm)	C_2 (K)
N_2	5.42e^{-5}	2.95e^{6}
O_2	7.12e^{-3}	1.91e^{6}
NO	4.86e^{-3}	1.37e^{5}

Table 2 Di-atomic species spectroscopic data.

Species	Fundamental frequency (Hz)	Characteristic temperature (K)
N_2	7.06e^{13}	3,390
O_2	4.72e^{13}	2,270
NO	6.41e^{13}	3,080

Species conservation equation

$$\frac{\partial(\rho Y_i)}{\partial t} + \nabla[u\rho Y_i] = -(\nabla . \mathrm{J_i}) + R_i + S_i \quad (7)$$

The total energy equation is altered by adding $\nabla \cdot [\Sigma_{i=1}^{n} h_i J_i]$ which represents energy associated with diffusion of species present in the reacting air.

$$\frac{\partial(\rho E)}{\partial t} + \nabla[u(\rho E)] + \nabla[\mathrm{u}p] + \nabla[T.u] + \nabla.j + \nabla.[\sum_{i=1}^{n} h_i J_i] = 0 \quad (8)$$

Here, total energy density, $\mathrm{E} = \mathrm{e} + \frac{1}{2}\mathrm{U}_2 + \Sigma_{\mathrm{i=1}}^{\mathrm{m}} \mathrm{Y_i} evib_i$, specific internal energy $e = c_v T$, diffusive heat flux $j = -k\nabla T$ (Fourier's law of heat conduction). Y_i is mass fraction of species $evib_i$ is the vibrational mode of energy per kg of di-atomic species and ρY_i gives partial density of species (ρs). $\nabla \cdot Ji$ Represents diffusion flux of species i due to concentration and thermal gradients.

$$J_i = (-\rho D_{im} \nabla \mathrm{Y_i}) + (-\frac{D_{T,i} \nabla \mathrm{T}}{\mathrm{T}}) \quad (9)$$

Here, the first term represents the diffusion of the species due to concentration gradients in the flow field. This term is derived from Fick's law. The diffusion coefficient Dim can be evaluated by the help of Schmidt number. The second term is due to diffusion of species due to presence of thermal gradient. As for simplifying the analysis, this term is dropped in the present study as this produces insignificant changes in the flow field.

R_i accounts the rate of formation or destruction of species due to chemical reactions which can be calculated by the help of law of mass action, while S_i is the external source term for representing catalytic surface. This term is insignificant for the present study as no such surface has been considered.

Finite volume method

In the finite volume methodology, the entire computational domain is divided into finite, discrete cells. The governing equations described above are applied on these cells and integration is performed under the limits of the cell. This procedure leads to conversion of governing equations in differential form to be converted into algebraic equations which can be solved simultaneously with the help of computers to obtain values in the centre of cells. The volume integral of divergence and gradient terms in the governing equation can be represented in terms of surface integrals by the help of Gauss divergence theorem. The surface integrals physically represent fluxes which can calculated approximately at each of the faces of the cell (control volume). The values at the faces of control surface can be evaluated by the help of interpolation and limiters which will be described in the upcoming sections. In the present study, Advection Upstream Splitting Method (AUSM) [3], Kurganov-Tadmor (K-T) [5] and its variant Kurganov-Noelle-Petrova (KNP) [6] scheme are used for convective flux calculation.

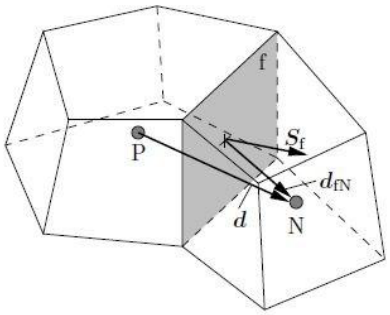

Figure 1 General schematic of a finite volume polyhedral cell.

The finite volume polyhedral cell is a co-located system with all dependent variable properties stored at cell centroid P. S_f is an area vector normal to the face surface pointing out of the owner cell, d connects centroid of cell, P with that of neighboring cell N and d_{fN} connects the center of the face to the centroid of the cell N. Discretization methods of temporal, convective, gradient and diffusion terms are explained in the subsequent sections

Temporal discretization

The term representing time dependence of variable is discretized using Euler explicit scheme. Finite volume method used for a general variable Ψ is as follows:

$$\int_V \frac{\partial(\rho\Psi)}{\partial t} dV \approx \frac{(\rho\Psi V)^{n+1} - (\rho\Psi V)^n}{\triangle t} \tag{10}$$

Spatial discretization

Central scheme

This is handled by the K-T and KNP schemes present in the rhoCentralFoam solver in OpenFOAM. Discretization using Finite Volume Method for convective term in governing equation for a general quantity is as follows:

$$\nabla \int_V \nabla.[u\Psi]dV = \int_S dS.[u\Psi] \approx \Sigma_f S_f \Psi_f = \Sigma_f \phi_f \Psi_f \tag{11}$$

where, $\phi_f = S_f u_f$ gives volumetric flux.

The flux values at cell interfaces can be obtained by interpolation of cell centre values (owner and neighbour) onto the faces. The interpolation is performed either using Upwind method or Central Differencing styles. In upwind schemes, information is interpolated from cells belonging to the upstream direction. Whereas, in central schemes (linear schemes) equal weightage for both the cells i.e. owner and neighbour is given. Linear and Upwind interpolation can be performed using weighting coefficient, $\omega_f = |S_f d_{fN}|/|S_f d_f|$ and flux of a dependent variable can be determined (using **Figure 1**) from the relation:

$$\Psi_f = \omega_f \Psi_P + (1 - \omega_f)\Psi_N \tag{12}$$

In compressible flows, information from one end is transferred to the other end not only by the transport of fluid but also due to propagation of disturbance wave in the convecting fluid medium. So the interpolation method employed needs to be split in 2 parts based on wave propagation direction, as *f*+ and *f*−. So, convective term discretization for a general variable can be written in this format.

$$\Sigma_f \phi_f \Psi_f = \Sigma_f [\alpha \phi_{f+} \Psi_{f+} + (1 - \alpha)\phi_{f-} \Psi_{f-} + \omega_f (\Psi_{f-} - \Psi_{f+})] \tag{13}$$

In this equation, the third term represents an additional term for providing dissipation with a volumetric flux ω_f based on the maximum propagation speed of the discontinuity present at an interface.

In the K-T scheme, equal weightage is given for fluxes interpolated from both the owner cell and neighbour cell. Hence, the weighting coefficient α = 0.5 is used, making this scheme a central scheme. In KNP scheme, the coefficient α is calculated in a manner giving high weightage to the cell in the upstream direction rendering the scheme to be central-upwind scheme. Volumetric fluxes based on local speed of propagation are determined by using these formulae mentioned below.

$$\Psi_{f+} = \max(c_{f+}|S_f| + \phi_{f+}, c_{f-}|S_f| + \phi_{f-}, 0) \tag{14}$$

$$\Psi_{f-} = \max(c_{f+}|S_f| - \phi_{f+}, c_{f-}|S_f| - \phi_{f-}, 0) \tag{15}$$

Here, $c_{f+} = \sqrt{\gamma RT_{f+}}$ and $c_{f-} = \sqrt{\gamma RT_{f-}}$ are the speeds of sound at the cell face determined by the help of owner and neighbour cell, respectively.

$$\alpha = \begin{cases} 0.5, & KT\ method; \\ \frac{\Psi_{f+}}{\Psi_{f+} + \Psi_{f-}}, & KNP\ method \end{cases} \tag{16}$$

The term representing dissipation in Eq. 7 can be evaluated by the following expressions.

$$\omega_f = \begin{cases} \alpha \max(\Psi_{f+}, \Psi_{f-}), & KT\ method; \\ \alpha(1-\alpha)\max(\Psi_{f+}, \Psi_{f-}), & KNP\ method \end{cases} \tag{17}$$

The KNP and K-T schemes as discussed above were implemented in rhoCentralFoam solver in OpenFOAM as such by Greenshields *et al.* [4].

Upwind scheme

One of the most commonly employed upwind schemes in the CFD community is Advection Upstream Splitting Method (AUSM) [4]. This scheme is simple, easy to implement and is able to capture discontinuities effectively and more so for shock discontinuities. The scheme is explained in detail using 1-Dimensional spatial discretization solving Euler's equation however, this can be extended to solve in other directions as well. The equations and terminology has been referred from Liou and Steffen [3]. The 1-Dimensional Euler's equation in conservative form can be written in this way [3],

$$\frac{\partial U}{\partial t} + \frac{\partial F}{\partial x} = 0 \tag{18}$$

Here, $U^T = (\rho, \rho u, \rho E)$, $F^T = (\rho, \rho u^2 + p, \rho uH)$, $E = e + 0.5u^2 = H - {}^{p}/_{\rho}$

The Flux Vector F can be split into 2 parts i.e. convective fluxes and pressure flux.

$$F = \begin{pmatrix} \rho \\ \rho u \\ \rho H \end{pmatrix} u + \begin{pmatrix} 0 \\ p \\ 0 \end{pmatrix} = F^{(C)} + \begin{pmatrix} 0 \\ p \\ 0 \end{pmatrix} \tag{19}$$

This convective flux vector is needed to be evaluated at the interface of the 2 cells. For the sake of avoiding redundancy, only calculations at the interface are discussed. The states at the left and right of the interface (denoted by 1/2) of the cells as *f*+ and *f*−, respectively.

$$F^{(C,1/2)} = u_{1/2} \begin{pmatrix} \rho \\ \rho u \\ \rho H \end{pmatrix}_{(f-/f+)} = M_{1/2} \begin{pmatrix} \rho a \\ \rho a u \\ \rho a H \end{pmatrix}_{(f-/f+)} \tag{20}$$

The values of conservative variables from cell centres on the interface is interpolated linearly based upon the interface Mach number ($M_{1/2}$). Mathematically,

$$(.)_{(f-/f+)} = \begin{cases} (.)_{(f-)}, & if\ M_{1/2} \geq 0 \\ (.)_{(f+)}, & otherwise \end{cases} \tag{21}$$

The interface Mach number ($M_{1/2}$) can be calculated from the following splitting

$$M_{1/2} = M_{f-} + M_{f+} \tag{22}$$

$$M^* = \begin{cases} \pm\frac{1}{4}(M \pm 1)^2, & if\ |M| \le 1; \\ \frac{1}{2}(M \pm |M|), & otherwise \end{cases} \tag{23}$$

The flux associated with pressure is also split based upon the following formulation

$$p_{1/2} = p_{f+} + p_{f-} \tag{24}$$

$$p^* = \begin{cases} \pm\frac{p}{4}(1 \pm |M|), & if\ |M| \le 1; \\ \pm\frac{p}{2}(M \pm |M|)/M, & otherwise \end{cases} \tag{25}$$

Interestingly, this upwind scheme can also be expressed in the following format of central scheme:

$$\begin{pmatrix} \rho u \\ \rho uu+p \\ \rho uH \end{pmatrix}_{1/2} = M_{1/2}\left[\begin{pmatrix} \rho a \\ \rho aU \\ \rho aH \end{pmatrix}_f + \begin{pmatrix} \rho a \\ \rho aU \\ \rho aH \end{pmatrix}_{f_+}\right] - \frac{1}{2}|M_{1/2}|\Delta_{1/2}\begin{pmatrix} \rho a \\ \rho aU \\ \rho aH \end{pmatrix} + \begin{pmatrix} 0 \\ p_{f+}+p_{f-} \\ 0 \end{pmatrix} \tag{26}$$

For the purpose of obtaining results, the pre-built AUSM solver in ANSYS Fluent 16.0 is used.

Limiters

The first order accurate discretization schemes are found to be stable, bounded (non-oscillatory) and diffusive (inaccurate), while second order schemes are more accurate but become unbounded when applied to convection dominated flow with bigger gradients. To prevent these oscillations with higher order discretization schemes, we add slope or gradient limiter function (r). Where, *r* represents the ratio of successive gradients of interpolated variable and *r* should be ≥ 0. Usage of limiters facilitates switching between lower and higher order schemes based on gradients. The limiter switches from higher order to lower order scheme, when it detects sharp gradients and vice versa. With the addition of appropriate limiter, it is possible to obtain required higher order and bounded scheme. These types of schemes are referred as "Total Variation Diminishing (TVD)" scheme. For a polyhedral mesh, the "*r*" for f_+ direction is given by:

$$r = \frac{2\ d.(\nabla\Psi)_P}{(\nabla_d\Psi)_f} - 1 \tag{27}$$

where, $(\nabla\Psi)_P$ is the gradient calculated with linear interpolation method at the owner cell P and $(\nabla\Psi)_f$ is the gradient normal to the face which is equal to $\Psi_N - \Psi_P$.

Different kind of limiters are used normally. In this study, the Van-Leer limiter and Superbee Limiter have been used. The Van-Leer limiter gives an optimum balance between stability and accuracy. It was found from [30] that for fine grid spacing, the Superbee limiter is significantly more accurate than Van-Leer and the oscillations decreased with a finer grid size.

Gradient terms

Discretization of the gradient term in governing equation using Finite Volume framework is as follows:

$$\int_V \nabla\Psi dV = \int_S dS\Psi \approx \Sigma_f S_f \Psi \tag{28}$$

Diffusive terms

The discretization using Finite Volume Method can be carried out as:

$$\int_V \nabla.(\tau \nabla\Psi)dV = \int_S dS(\tau \nabla\Psi) \approx \Sigma_f \tau_f S_f(\nabla\Psi)_f \quad (29)$$

where, τ_f can be calculated by linear interpolation from neighbour cell centred values.

Results and discussion

In this section, the evaluation and comparison for 2 classes of schemes - the Upwinding and Central schemes; Advection Upstream Splitting Method for the former and, Kurganov-Noelle-Petrova and Kurganov-Tadmor for the latter are carried out. To compare them, the problems chosen are typical inviscid problems encountered in compressible flows. The analysis is carried out using the inbuilt AUSM solver in ANSYS Fluent 16.0 for implementing AUSM scheme and for KNP and K-T schemes, the rhoCentralFoam solver used in OpenFOAM version 3.0.1. [4].

The first case is Sod's 1-Dimensional Shock Tube case [8]. The second problem took the forward facing step case which was simulated by Woodward and Collella [9]. The third set took the case of a 15 degree ramp from John *et al.* [2]. The fourth problem involved a Mach Reflection as shown by Ben-Dor and Takayama [11]. Finally, the fifth problem was a Mach 5 flow through a scramjet engine.

First a comparison between these schemes is made in Sod's 1-Dimensional Shock Tube Case [8]. This is problem of unsteady wave motion occurring inside a channel. Initially, the 2 states of unequal pressure of a gas are separated denoted by L and R is separated by a diaphragm. The high pressure gas is on the left side and low pressure gas on the right side. As soon as the diaphragm is broken, the shock wave travels into the low pressure region and the expansion wave traverses in the high pressure region. A contact discontinuity (moving slip line) is formed between the shock wave and the expansion wave. To simulate this physics, Sod's shock tube problem has been utilized. The states on the left side of the diaphragm are denoted by L as, ρ_L = 1.0 kg/m^3, p_L = 100,000 Pa, T_L = 348.4 K and states on the right side are denoted by R as, ρ_R = 0.125 kg/m^3, p_R = 10,000 Pa, T_R=278.7 K. Air having gas constant R = 287 J/kg. K is modelled as an ideal gas. The total length of the tube is 10 m with a diaphragm located at the middle of the tube. The domain is in the range between −5 and 5 m. There are 3 objectives for this study, the first is a comparison between K-T and KNP scheme to find the better central-differencing scheme, the second to find out whether a grid-independent study is possible, and finally a comparison between the better central differencing scheme and AUSM scheme. For the purpose of the study, the density plot obtained at t = 7 ms is obtained and a Courant-Friedrichs-Lewy (CFL) number of 0.2 is utilized for obtaining stable calculations.

Comparison between central-differencing schemes

A fine mesh of 1,000 cells in x-direction is utilized to obtain solution using both the K-T and KNP schemes as shown in **Figure 2**. It is observed that the KNP scheme solution displays oscillations after the shock discontinuity whereas the K-T scheme shows no such instabilities. When further refinement of the mesh was carried out, the oscillations increased for the KNP scheme, whereas for K-T scheme, it remained the same. Therefore, the K-T scheme has been selected for further study.

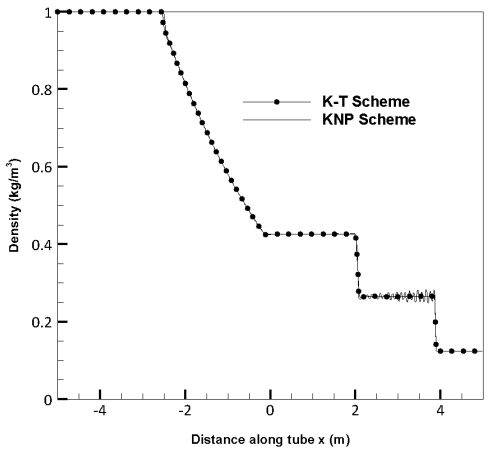

Figure 2 Comparison between K-T and KNP schemes.

Comparison between K-T and AUSM scheme

The density variation obtained by solving Euler equation using AUSM and Kurganov-Tadmor scheme for convective flux discretization is obtained and compared with the analytical solution and is shown in **Figure 3**. Both schemes are robust enough to capture all the 3 features that may occur in the compressible flow problems, i.e. shock, contact and expansion. However, there is a notable difference present in the contact discontinuity at x = 2 m captured by AUSM and K-T schemes. The contact discontinuity captured by AUSM scheme appears to be slightly dissipative as compared to K-T scheme. Another feature of the flow field, i.e. the normal shock discontinuity captured by AUSM scheme required a marginally higher number of cells as compared to K-T scheme suggesting dissipative nature of AUSM scheme. The expansion was simulated equally well by both of these schemes. This 1-dimensional simulation suggests the dissipative nature of AUSM scheme, especially for contact discontinuities. To assess this comparison further, the 2-dimensional case of a forward step in a supersonic wind tunnel is simulated and is presented next.

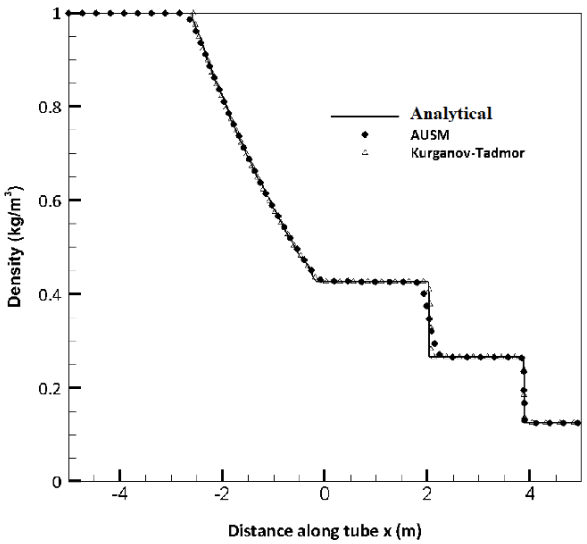

Figure 3 Comparison between analytical solution, K-T and AUSM schemes.

Flow over a forward step in a Mach 3 supersonic tunnel

This supersonic flow problem starts with a forward-facing step in supersonic Mach 3 tunnel. The tunnel's height is 1 unit and length is 3 units. The forward-facing step is 0.2 length units high and is situated 0.6 units from the left side of the tunnel. The tunnel here is assumed to be in infinite length in breadthwise direction which restricts the problem to be in 2-dimensions. At the left of the tunnel supersonic free stream conditions are imposed as boundary conditions. The inlet velocity is 3 and speed of sound is unity. The temperature and pressure values are assumed to be unity. On the right side, all gradients for the variables being solved are vanished. This is because the exit boundary conditions have no effect on the flow field as exit velocity is supersonic. Initially the tunnel is filled with gas having ratio of specific heats equal to 1.4 and pressure, temperature and velocity initialized to free stream condition. The gas behaves as an ideal gas and hence from the calculations the density of the gas is ρ = 1.4 kg/m^3. The walls of the boundary are reflecting. The time evolution of the flow field up to t = 4 s are presented obtained by both of these schemes. A qualitative comparison is made between the results obtained here and those obtained by Woodward and Collella [9]. The computational grid used in the present study is of 80×240 cells for both convective flux discretization schemes.

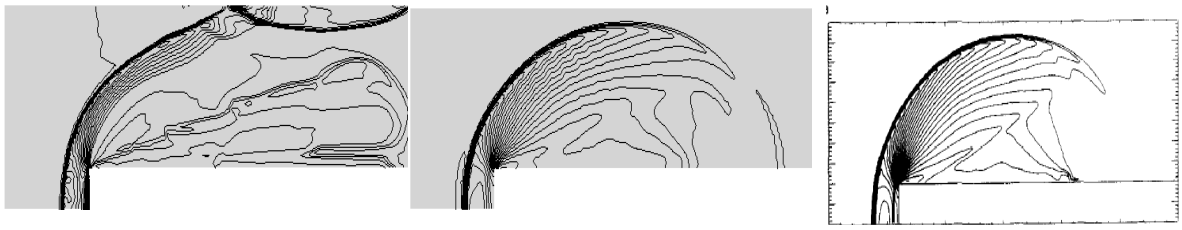

(a) (b) (c)

Figure 4 Normalized density at t = 0.5 s using (a) AUSM, t = 0.5 s, (b) K-T, t = 0.5 s, (c) Woodward and Colella [9] at t = 0.5 s.

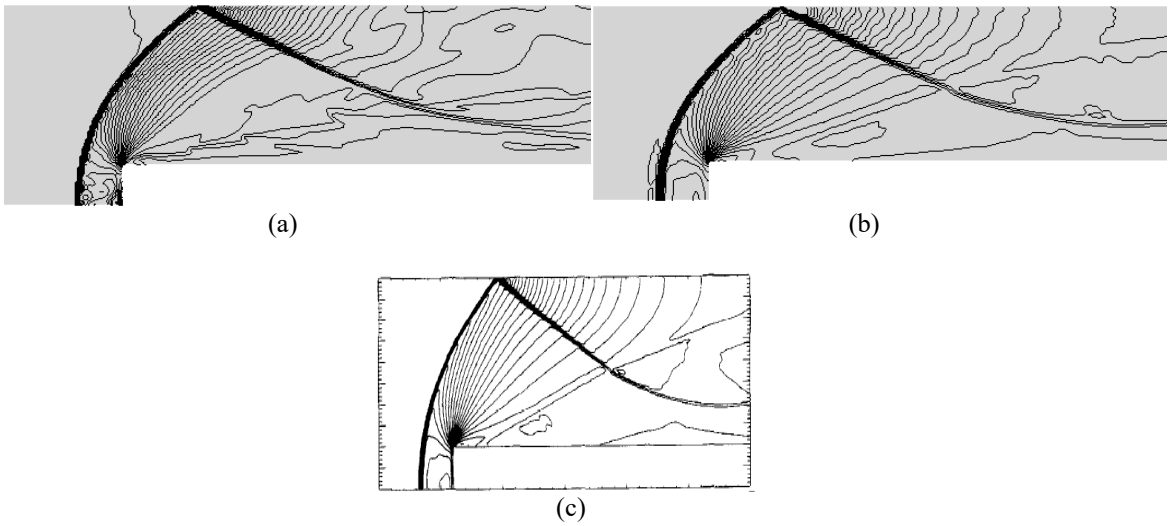

(a) (b)

(c)

Figure 5 Normalized density at t = 1 s using (a) AUSM, t = 1 s, (b) K-T, t = 1 s, (c) Woodward and Colella [9] at t = 1 s.

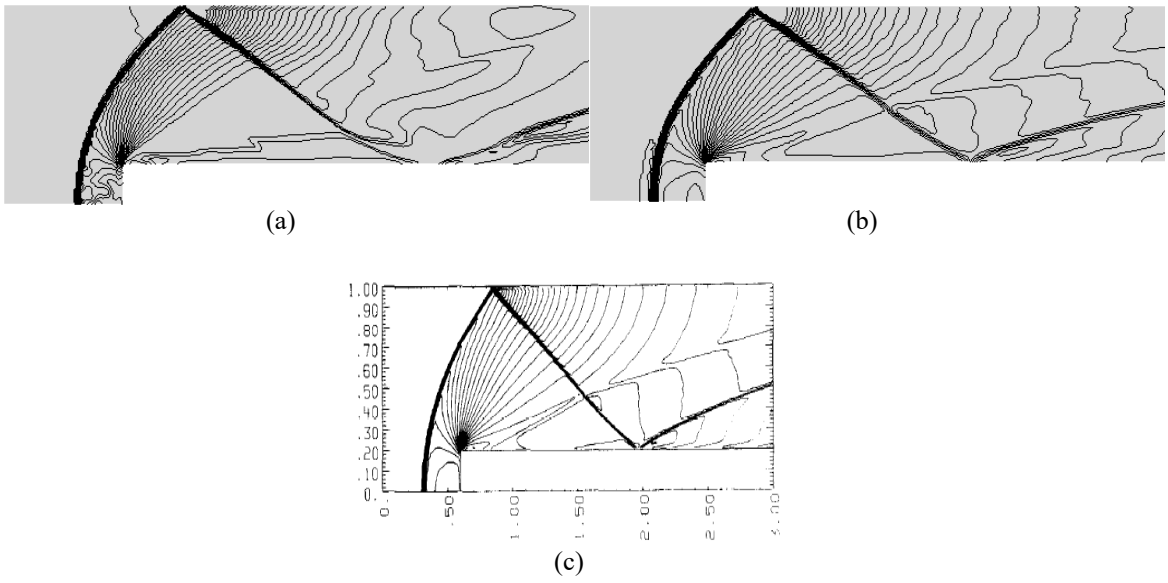

(a) (b)

(c)

Figure 6 Normalized density at t = 1.5 s using (a) AUSM, t = 1.5 s, (b) K-T, t = 1.5 s, (c) Woodward and Colella [9] at t = 1.5 s, density contours (0.8:0.2:9.0).

The flow field in form of normalized density contour is obtained using AUSM, K-T and Woodward and Colella [9] results at various instances of time starting at t = 0.5 s and ending at t = 4 s is depicted in the **Figures 4 - 11**. The supersonic flow in the wind tunnel experiences a blunt obstacle which results in formation of bow shock in front of it. In this process the flow is deviated from its original course and hence, a series of reflections of the oblique shocks from the wall are seen. The first reflection occurs on the upper wall. This reflection is not a regular reflection but a Mach reflection. The reflected shock from this position hits on the upper side of the obstacle and again this shock is reflected back to the top wall and it finally exits from the tunnel. This shock structure evolution using Kurganov-Tadmor scheme is in similar lines as reported by Woodward and Colella [9].

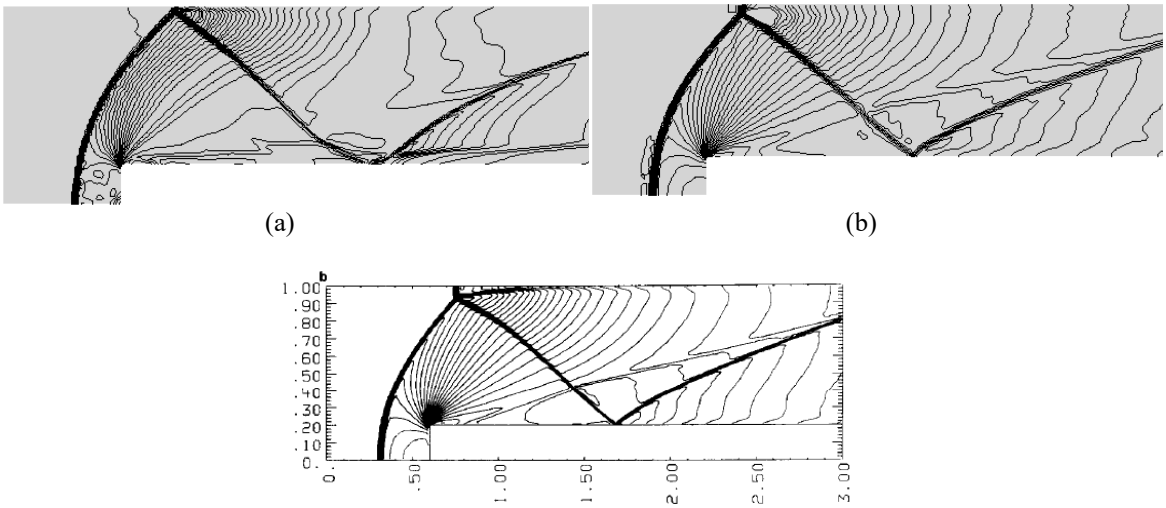

(a) (b)

(c)

Figure 7 Normalized density at t = 2 s using (a) AUSM, t = 2 s, (b) K-T, t = 2 s, (c) Woodward and Colella [9] at t = 2 s.

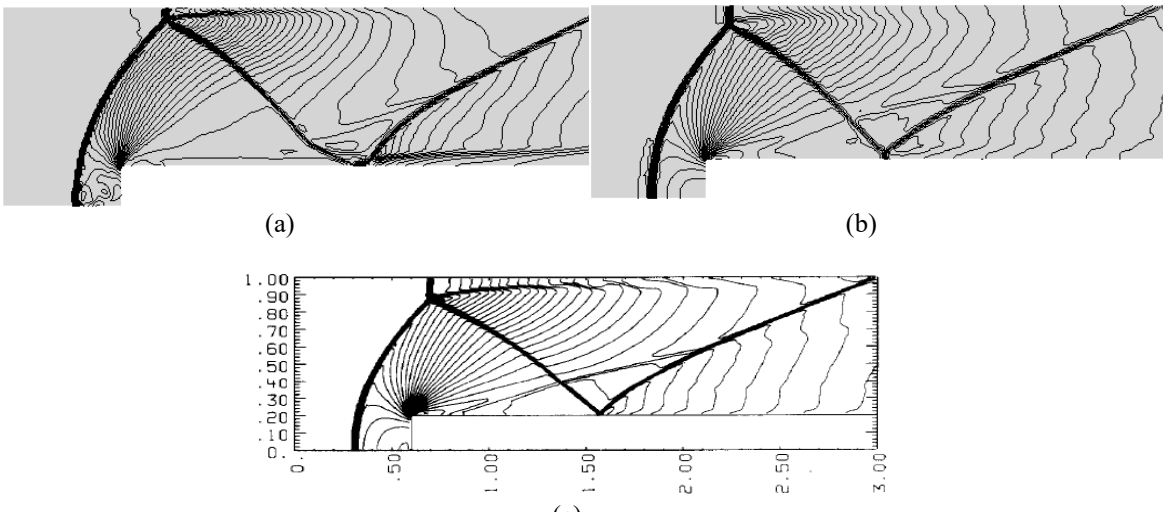

(a) (b)

(c)

Figure 8 Normalized density at t = 2.5 s using (a) AUSM, t = 2.5 s, (b) K-T, t = 2.5 s, (c) Woodward and Colella [9] at t = 2.5 s.

However, the shock pattern at t = 0.5 s using AUSM scheme deviates from the results by Woodward and Colella [9]. According to this literature, for some schemes an additional boundary fix is required at the point of singularity at the corner of the forward step since it is the centre of a rarefaction fan.

Consequently, some numerical schemes may generate large numerical errors. These errors generate a boundary layer which is approximately 1 zone thick just above the top surface of the step which is seen in the contours obtained using AUSM scheme. The impinged shock then interacts with this boundary layer altering the flow field more or less dramatically. The sensitivity of this singular point is dependent upon the numerical scheme employed for the solution. Therefore, to minimize the flow alteration due to this numerical error, an additional fix in the form of boundary conditions is required to be implemented. To implement this, the first row of cells above the wall of the step, the first 4 cells starting from the right of the corner and 2 cells above this row is reset after every iteration. The density here is re-initialized so the entropy in the cells left and below the corner has same values. The velocity magnitude is also reset but the direction is not, so, the total enthalpy per unit mass has the same value as the cells utilised to reset the entropy. This boundary condition is based on the conjecture of almost steady flow in the region near corner of the step. This boundary condition may however result in overexpansion which is almost similar to the effects produced in supersonic wind tunnel using real, viscous gas.

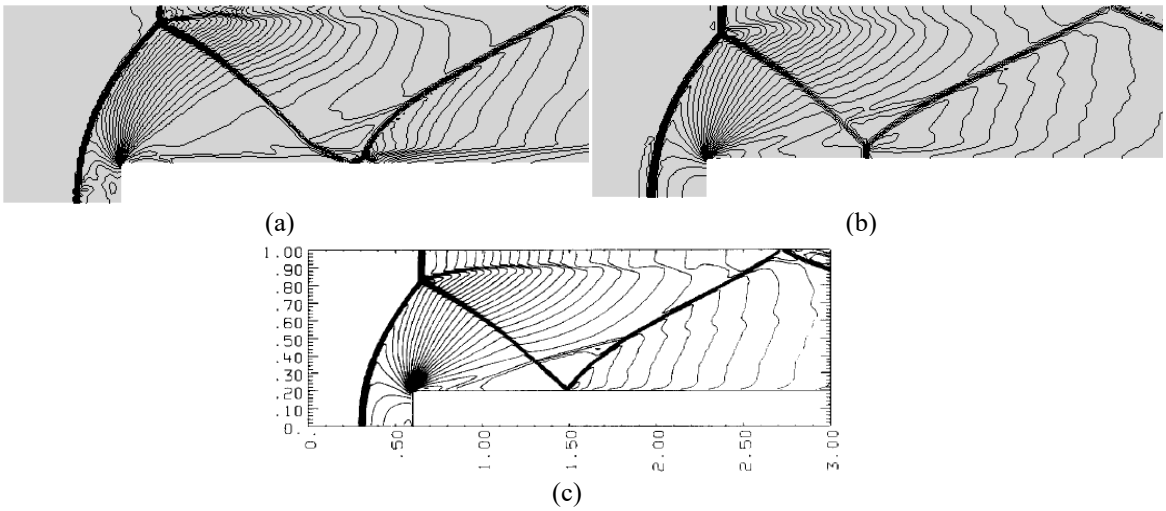

Figure 9 Normalized density at t = 3 s using (a) AUSM, t = 3 s, (b) K-T, t = 3 s, (c) Woodward and Colella [9] at t = 2.5 s. Density contours (0.8:0.2:9.0).

Here in the present study the entropy fix in the form of boundary condition mentioned above was not implemented for any scheme. The discrepancies in the results obtained using AUSM scheme, and results obtained by Woodward and Colella [9] can be clearly seen qualitatively from contour plots whereas minute differences in the results are observed obtained using K-T scheme. This is attributed to higher order of accuracy of the K-T scheme but due to this higher order of accuracy, the flow on the top face of the step is prone to dispersion (oscillation) due to sudden turning of the flow field around the corner of the step. To handle this, the generic scheme for total variation diminishing (TVD) limiting of the vector field (V-scheme) is used and it results in a stability against these oscillations.

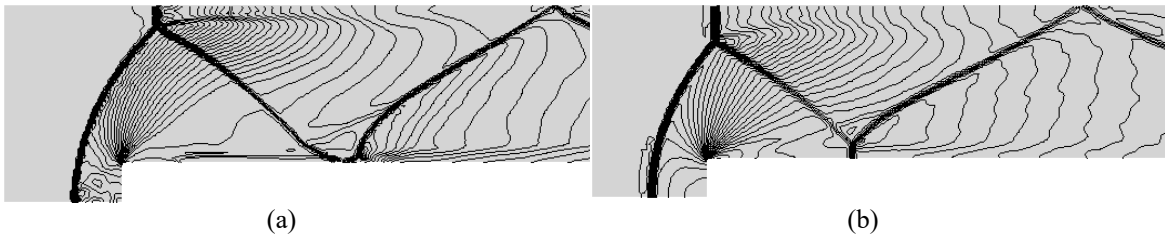

Figure 10 Normalized density at t = 3.5 s using (a) AUSM, t = 3.5 s, (b) K-T, t = 3.5 s.

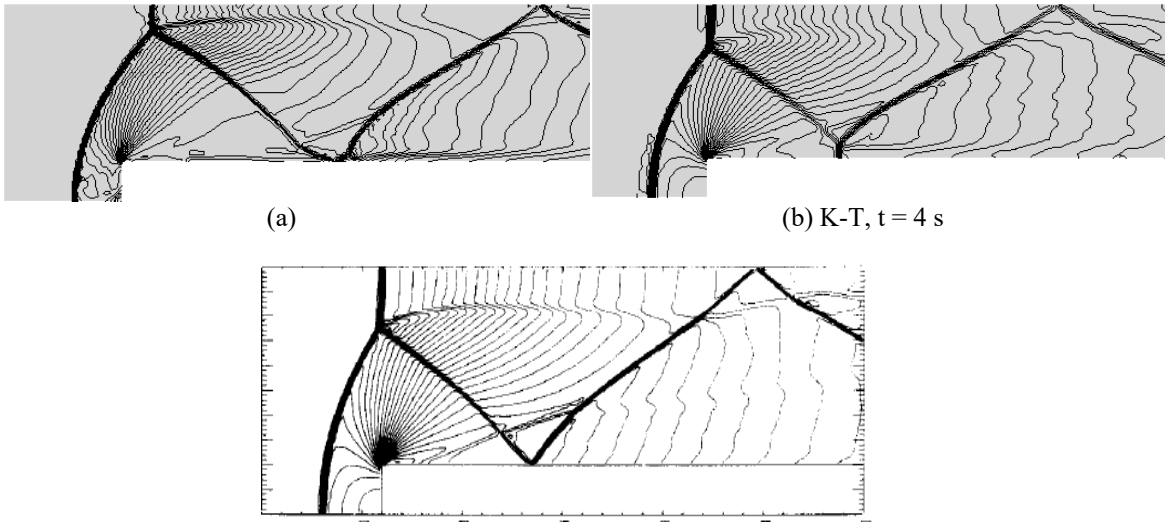

(a) (b) K-T, t = 4 s

(c)

Figure 11 Normalized density at t = 4 s using (a) AUSM, t = 4 s, (b) K-T, t = 4 s, (c) Woodward and Colella [9] at t = 4 s, density contours (0.8:0.2:9.0).

The Kurganov-Tadmor scheme did not require any special entropy fix as it is second order accurate but a velocity limiter is required to supress the oscillations, but AUSM requires additional boundary conditions as mentioned above to produce accurate results.

Mach 2 flow over a 15-degree ramp

The supersonic Mach 2 flow over a 15-degree ramp produces an attached shock at the compression corner. The ramp is in a supersonic tunnel which has a height of 1 unit and length of 3 units. The ramp is placed 0.5 units right of the inlet. The total length of the ramp is 0.5 units. The inlet of the tunnel has been exposed to supersonic free stream conditions. The wall and obstacle are inviscid and the exit boundary condition is maintained for 0 gradient as the exit doesn't have any influence on the flow field. This is because the exit velocity is always supersonic. This problem has been solved using non-dimensional methodology hence the pressure and temperature of the gas at the inlet is 1 unit each. The gas is gamma law gas with = 1.4 and follows ideal gas relation. The entire domain is initialized with free stream condition with density of $\rho = 1.4$ kg/m^3. The computational grid used in the present study is of 180×90 which is used for both of the schemes. The boundary conditions and domain dimensions are depicted in **Figure 12**.

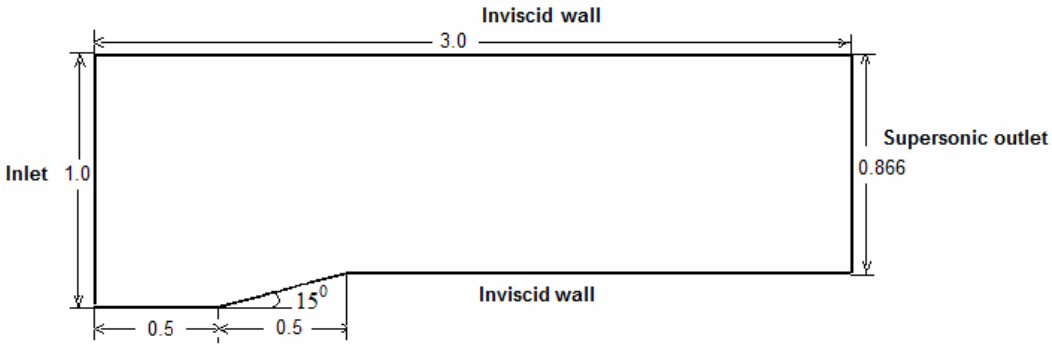

Figure 12 Domain and boundary condition for Mach 2 flow over a 15-degree ramp [10].

The supersonic flow in the tunnel experiences a ramp as an obstacle which is a compression corner. An attached oblique shock is formed at the compression corner and hits the top wall from where Mach reflection takes place. The flow crossing the Mach stem (having small height) has higher entropy as the

Mach Stem is a normal shock as compared to the flow passing through the 2 oblique shocks. Therefore, there is a slip line separating these 2 states emanating from the triple point i.e. the point of interaction of 2 oblique shocks and the Mach Stem. The reflected shock from the triple point again hits the top surface of the ramp's shoulder and exits the domain. The point of intersection of the ramp and shoulder portion serves as an expansion fan corner. The position of the shock reflection positions on the wall is dependent on the accuracy of the numerical convective discretization scheme employed. The **Figure 13** below shows qualitative contour plots of normalized density obtained using both the schemes. The solution is converged till steady state and residuals are in order of 10^{-4}.

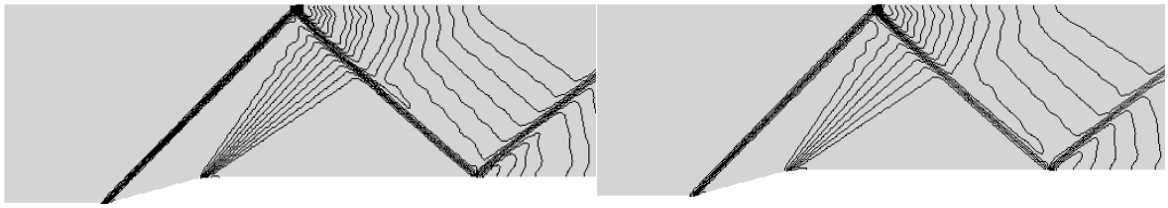

(a) (b)

Figure 13 Normalized density contours (1.4:0.1:4.5) using (a) AUSM scheme and (b) Kurganov- Tadmor scheme.

It is observed that the contour plots for both schemes are almost similar and therefore of similar accuracy for this particular problem. The non-dimensional plot obtained using these schemes are displayed in **Figure 14** and compared with the results obtained by Ganesh [10].

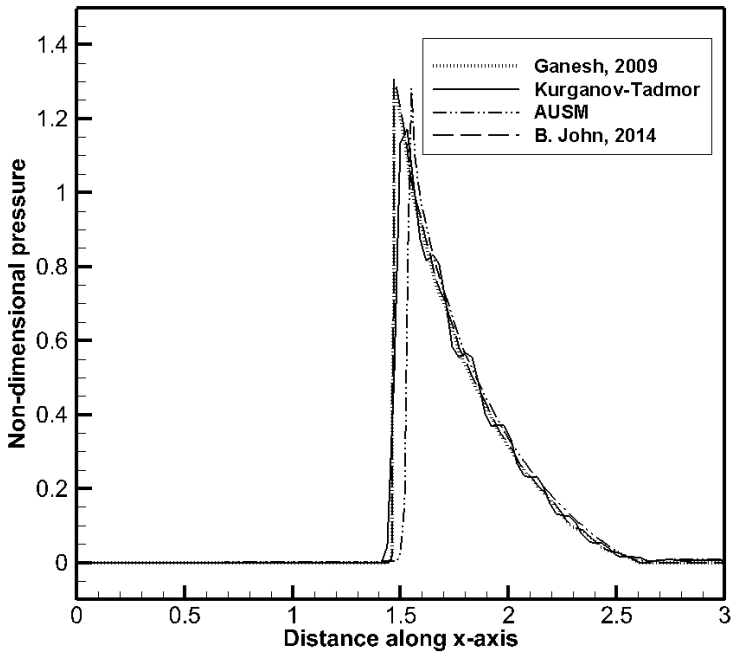

Figure 14 Wall pressure distribution and pressure rise across the Mach stem.

The rise of pressure as recorded by K-T scheme matches well with the results obtained by Ganesh [10]. The results obtained using AUSM scheme also follows the similar trend. The peak pressure rise obtained using both the schemes are under predicted with K-T scheme showing a lesser value as compared to AUSM scheme. The normal shock near x = 1.5 is captured more accurately in case of K-T

scheme but AUSM scheme gives dissipative results. The crisp normal shock structure captured by K-T scheme is credited to its higher order of accuracy. No anomalies of oscillatory behaviour are observed in case of pressure distribution using either scheme.

Mach reflection

The Mach reflection occurs when regular reflection from the boundary is not possible. This is because no solution for the wave angle exists for prevailing conditions and $\theta - \beta - M$ relation. In this situation, a "lambda" shock pattern is created where the normal shock and 2 oblique shocks interact. The flow passing through the normal shock portion of this structure experiences higher entropy change as compared to the flow passing through a series of oblique shocks. Hence, to differentiate between these 2 states, a slip line (SS) emanates from the triple point (T). The "lambda" shock structure is shown in below, **Figure 15**.

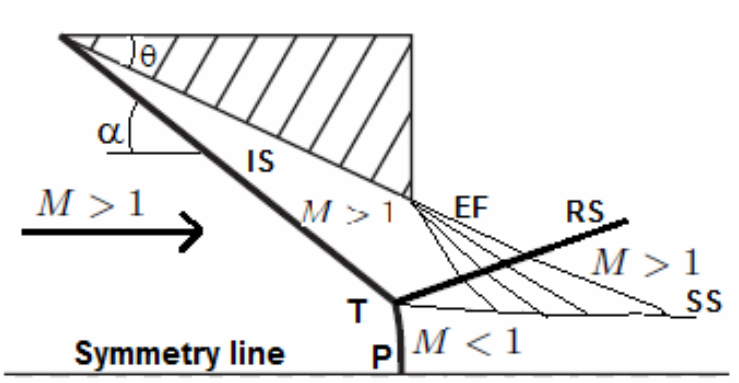

Figure 15 Flow structure of "lambda" shock [2].

The Mach stem height Hm (TP) as shown in **Figure 15** is a strong function of Mach number and wedge length l_w. In contrast to the earlier studies, the height of the Mach stem is prominent in this problem and for comparison purpose, the experimental results of Mouton and Hornung [12] and analytical results by Ben-Dor and Takayama [11] is utilized in the present study. The geometrical configuration used by Ben-Dor and Takayama [11] is utilized here with incident shock wave angle β = 40.7 degrees. The computational domain along with the boundary conditions are shown in **Figure 16**. The domain has been divided into approximately 40,000 cells. The free stream Mach number is 2.84 and the throat to wedge length ratio is 0.37. Both the numerical schemes are employed for calculating the solution to the problem. The contours of Mach numbers obtained by both the schemes is shown in **Figure 17**. The Mach stem and the slip lines using both the schemes is captured quite accurately.

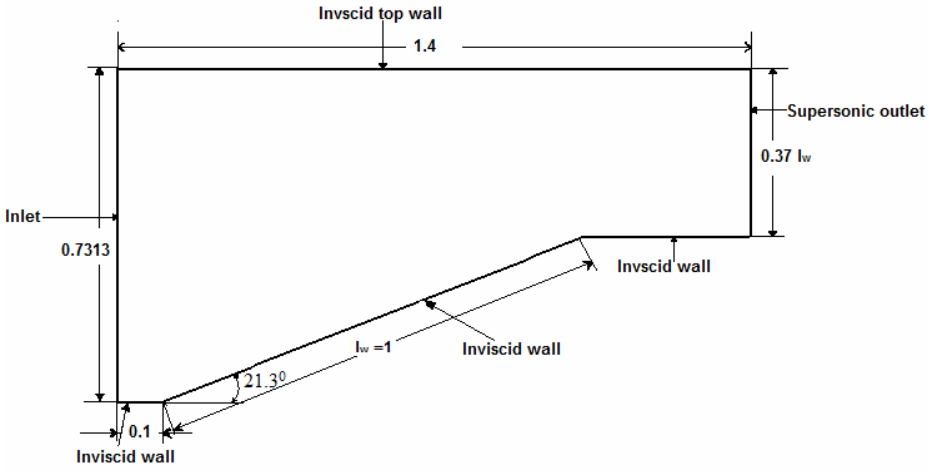

Figure 16 Computational domain and boundary conditions for Mach reflection [11].

The Mach stem height in **Figure 18** obtained using both the schemes is compared to previous available experimental and simulation results. It can be seen here that the height of the Mach stem is significantly overpredicted by both the schemes. However, the Mach stem height predicted using AUSM scheme is in close agreement to experimental and previous numerical results. The Mach stem height predicted by K-T scheme is slightly over predicted when compared with AUSM scheme. Both the schemes performed equally well.

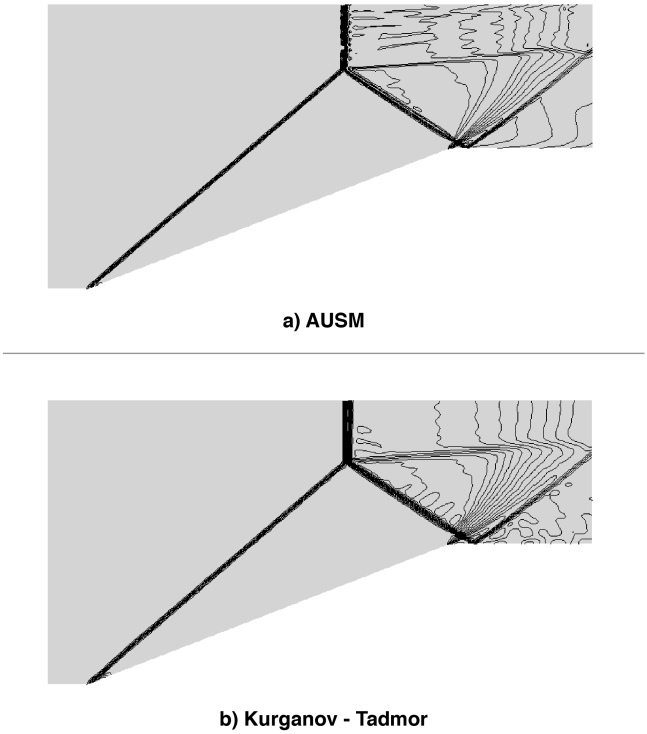

Figure 17 Density contour (0.2:0.2:6.2) using a) AUSM scheme and b) Kurganov-Tadmor scheme.

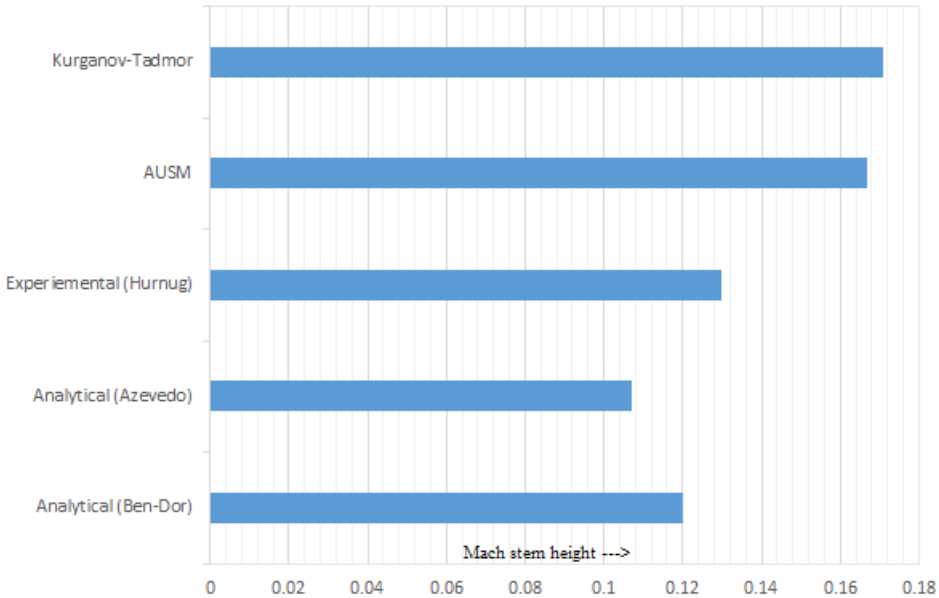

Figure 18 Comparison of Mach stem height obtained using AUSM scheme and Kurganov-Tadmor scheme with analytical and experimental results.

Mach 5 flow thorough scramjet engine

The last problem utilized for the purpose of convective flux scheme performance evaluation is the supersonic combustion ramjet engine or scramjet engine. This particular case is considered to be operating in the hypersonic range. Hence a Mach 5 flow through this scramjet engine is considered here. This configuration was utilized earlier by Kumar [13] and the same configuration is utilized over here for the purpose of flux scheme evaluation. The flow structure inside this model is quite complex as a lot of interactions like oblique shocks, emanating from various compression corners, expansion fans from different expansion corners in domain, interaction of shocks on the symmetrical line, shock reflection from the wall, interactions of shock and expansion waves and slip lines separating 2 different states of fluid but with the same pressure are observed. The computational grid utilized here has around 20,000 cells. The non-dimensional density contours shown in **Figure 19** obtained by both schemes qualitatively agree with the results shown in Kumar [13]. Crisp shocks and all other flow structures are captured by both K-T and AUSM. The centre line non-dimensional density plot shown in **Figure 20** obtained using both the schemes suggests comparable performance of both the schemes.

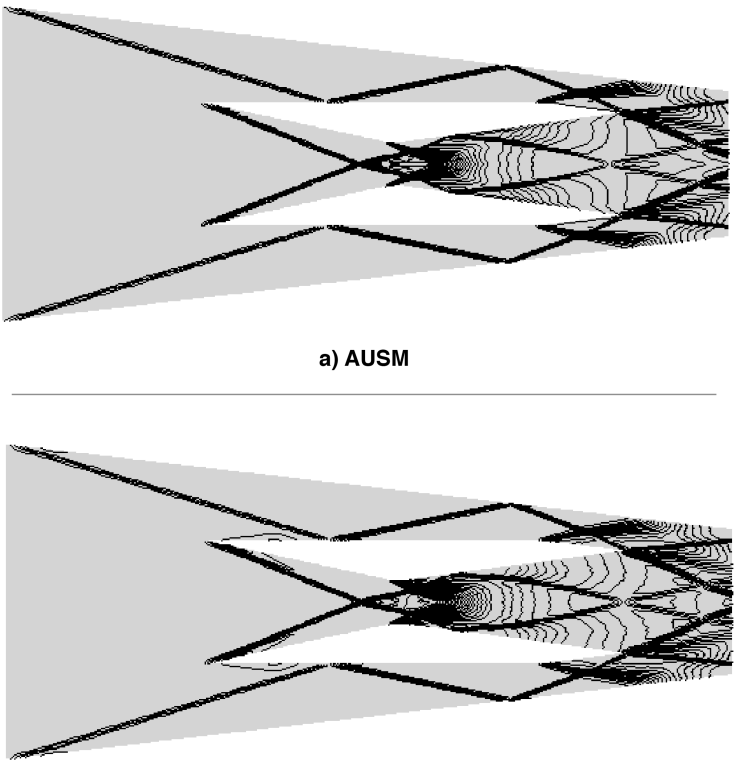

Figure 19 Non-dimensional density contours (1.1:0.24:7.8) in the scramjet engine.

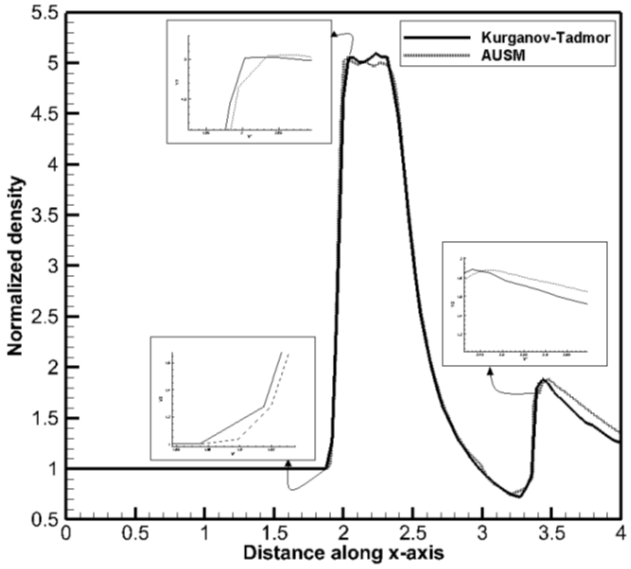

Figure 20 Centre line density plot of the scramjet engine.

From the results obtained from the above cases, it is evident that both the discretization schemes are robust enough to capture all features of the compressible flows. The AUSM scheme was found to be more dissipative as compared to K-T while capturing the contact discontinuity. However, the normal shock discontinuity was captured accurately by both the schemes. The state the fluid attained after crossing the normal shock, when captured by K-T scheme was prone to oscillations with visible ”wiggles” in the line plot as well as the contour plots of the field variables. This indicates a dispersive nature for the K-T scheme, contrary to the dissipative nature of the AUSM scheme.

Conclusions

In this work, a comparison has been carried out between the two convective flux discretization techniques i.e. the upwind scheme of AUSM and the central schemes of K-T and KNP. Inviscid simulations for various problems in the supersonic as well as hypersonic regime were used to carry out this comparison. The conclusions are as follows:

(1) For Sod’s 1-Dimensional Shock Tube, when KNP scheme was used, it was found that after the shock discontinuity, oscillations where exhibited which increased in amplitude on further refinement of the mesh. The K-T scheme however, displayed no such “wiggles” in its solution. When comparing K-T with AUSM scheme for Sod’s 1-Dimensional Shock tube, all the flow features of compressible flow are captured equally well. However, the contact discontinuity was dissipative for AUSM as compared to Kurganov-Tadmor scheme.

(2) Certain anomalies can be observed in the case of flow over forward facing step in supersonic wind tunnel using AUSM scheme. This was attributed to the gross numerical error generated at the singular point (corner of forward step). This suggests special treatment in the form of isentropic boundary condition for this singular point was needed but no special treatment was used for simulating the same case using Kurganov-Tadmor scheme. In the same problem of supersonic flow in a forward facing step, Kurganov-Tadmor scheme produced an oscillatory velocity field due to its dispersive nature and hence a Van-leer flux limiter for momentum convective flux was required to stabilize the solution.

(3) For the Mach 2 flow over a 15-degree ramp, similar normalized density contour plots were obtained for both schemes. However, peak pressure for K-T scheme is found to be lesser than that for AUSM scheme and the shock was captured more accurately by the K-T scheme.

(4) For the Mach Reflection problem, the height of the mach stem is overpredicted by both schemes, with AUSM being closer to experimental and previous numerical results. The K-T scheme also shows dissipation after the second shock.

(5) For Mach 5 flow through a Scramjet Engine, both schemes were robust enough to capture the flow features accurately.

(6) From the results, it can be seen that both schemes perform equally in capturing the flow features, with K-T having more accuracy for the Sod's shock tube, Forward facing step problem and 15 degree ramp. However "wiggles" were seen for K-T scheme for the Mach Reflection problem. This is because the scheme is even order (second order) accurate and dispersive in nature.

References

[1] JD Anderson. *Modern compressible flow*. Mcraw Hill, New York, 2003.
[2] B John, G Sarath, V Kulkarni and G Natarajan. Performance comparison of flux schemes for numerical simulation of high-speed inviscid flows. *Prog. Comput. Fluid Dynam. Int. J.* 2014; **14**, 83-96.
[3] MS Liou and CJ Steffen. A new flux splitting scheme. *J. Comput. Phys.* 1993; **107**, 23-39.
[4] CJ Greenshields, HG Weller, L Gasparini and JM Reese. Implementation of semi-discrete, non-staggered central schemes in a colocated, polyhedral, finite volume framework, for high-speed viscous flows. *Int. J. Numer. Meth. Fluid.* 2010; **63**, 1-21.
[5] A Kurganov, S Noelle and G Petrova. Semidiscrete central-upwind schemes for hyperbolic conservation laws and Hamilton-Jacobi equations. *SIAM J. Sci. Comput.* 2001; **23**, 707-40.
[6] A Kurganov and E Tadmor. New high-resolution central schemes for nonlinear conservation laws and convection diffusion equations. *J. Comput. Phys.* 2000; **160**, 241-82.
[7] B van Leer. Towards the ultimate conservative difference scheme. II. Monotonicity and conservation combined in a second-order scheme. *J. Comput. Phys.* 1974; **14**, 361-70.
[8] GA Sod. A survey of several finite difference methods for systems of nonlinear hyperbolic conservation laws. *J. Comput. Phys.* 1978; **27**, 1-31.
[9] P Woodward and P Colella. The numerical simulation of 2-dimensional fluid flow with strong shocks. *J. Comput. Phys.* 1984; **54**, 115-73.
[10] N Ganesh. 2010, Residual error estimation and adaptive algorithms for compressible flows. Ph. D. Dissertation. Department of Aerospace Engineering, Bangalore, India.
[11] G Ben-Dor and K Takayama. The phenomena of shock wave reflection-a review of unsolved problems and future research needs. *Shock Waves* 1992; **2**, 211-23.
[12] CA Mouton and HG Hornung. Mach stem height and growth rate predictions. *AIAA J.* 2007; **45**, 1977-87.
[13] A Kumar. Numerical analysis of the scramjet inlet flow field using two-dimensional Navier-Stokes equations. *In*: Proceedings of the 19th Aerospace Sciences Meeting, Missouri, USA. 1981, p. 185.